

Large-scale structure in the Lyman- α forest – A new technique

J. Liske,¹ J. K. Webb¹ and R. F. Carswell²

¹*School of Physics, University of New South Wales, Sydney 2052, Australia.*

²*Institute of Astronomy, Madingley Road, Cambridge CB3 0HA, U.K.*

Accepted Received

ABSTRACT

We present a new technique for detecting structure on Mpc scales in the Ly α forest. The technique is easy to apply in practice since it does not involve absorption line fitting but is rather based on the statistics of the transmitted flux. It identifies and assesses the statistical significance of regions of over- or underdense Ly α absorption and is fairly insensitive to the quality of the data. Using extensive simulations we demonstrate that the new method is significantly more sensitive to the detection of large-scale structure in the Ly α forest than a traditional two-point correlation function analysis of fitted absorption lines.

Key words: large-scale structure of Universe – quasars: absorption lines

1 INTRODUCTION

Over the past few years new information has emerged that warrants a new investigation into the large-scale clustering properties of the Ly α forest seen in the spectra of distant QSOs. Observationally, major advances have been achieved with the help of the HST and the Keck telescope. At the lowest redshifts, where Ly α absorbers are probed by HST, multi-slit spectroscopy of galaxies in the fields of bright QSOs has resulted in the direct identification of galaxies which produce Ly α absorption, as evidenced by the anti-correlation between the Ly α equivalent width and the distance of the absorbing galaxy from the QSO sight-line (Chen et al. 1998; Lanzetta et al. 1995). The correlation appears to extend out to very large distances (Tripp, Lu, & Savage 1998), where the interpretation may be different and the Ly α absorber presumably may not be directly associated with the ‘identified’ galaxy. Regardless of the interpretation on any scale, it now seems clear that the number density of Ly α absorbers is larger in those regions of space where galaxies reside, and thus Ly α absorbers trace large-scale structure.

At high redshift, there is also mounting evidence that a significant fraction of Ly α absorbers is associated with (proto-) galaxies. The discovery of CIV in 75 per cent of absorbers with $N(\text{HI}) = 3.0 \times 10^{14} \text{ cm}^{-2}$ at $z \sim 3$ (Songaila & Cowie 1996) challenges the original interpretation of the Ly α forest as a primordial, randomly distributed, intergalactic population. Furthermore, Fernández-Soto et al. (1996) showed that Ly α lines with associated weak CIV absorption cluster strongly in redshift and they concluded that the observed clustering is broadly consistent with that expected for galaxies at $z \sim 2 - 3$ (but see also Songaila & Cowie 1996).

The high redshift observations may be understood theoretically and placed within the context of cosmological structure formation with the help of numerical simulations. Using a uniform metal enrichment of the IGM of $[\text{C}/\text{H}] \sim -2.5$, produced by a postulated Population III burst of star formation, Hellsten et al. (1997) found that they could reproduce the observed mean value of the CIV/HI ratio with numerical simulations of cosmological structure formation. However, the scatter of this ratio implied an inhomogeneous metallicity distribution in the IGM. Gnedin (1998) subsequently suggested that the dominant mechanism for the enrichment of the IGM is the merger mechanism which reproduces both the mean and scatter of the CIV/HI ratio.

In general, the simulations seem to suggest that Ly α absorbers are a less biased tracer of the underlying mass distribution than are galaxies (Cen et al. 1994; Miralda-Escudé et al. 1996; Cen & Simcoe 1997; Hernquist et al. 1996; Zhang, Anninos, & Norman 1995; Petitjean, Mückel, & Kates 1995; Mückel et al. 1996; Riediger, Petitjean, & Mückel 1998; Wadsley & Bond 1997; Bond & Wadsley 1998).

There is also direct observational evidence that the Ly α forest exhibits large-scale structure. Pando & Fang (1996) used

a discrete wavelet transform to perform a space-scale decomposition of the Ly α forest and to demonstrate the existence and evolution of clusters on scales as large as $20 h^{-1}$ Mpc. Recently, Williger et al. (1998) reported correlations of Ly α absorbers over $\sim 36 h^{-1}$ comoving Mpc in the plane of the sky at $2.15 < z < 3.37$.

Fitting individual absorption lines and computing their two-point correlation function (tpcf) is the most commonly adopted approach to clustering analysis of the Ly α forest. Pando & Fang (1996) discussed this and other methods based on line statistics and concluded that a space-scale decomposition is most effective. However, the analysis by Fernández-Soto et al. (1996) demonstrates the difficulty of using any sort of analysis based on the statistics of fitted absorption lines. Even in high resolution spectra blending successfully masks even very strong clustering, so that any procedure involving identifying individual absorption lines may severely underestimate the strength and scale of the ‘true’ correlation. In addition, if the aforementioned numerical simulations are more or less correct then at least the low column density forest does not correspond to well-defined individual ‘clouds’ since it arises in a fluctuating but continuous medium with small to moderate overdensities.

Ideally we therefore need a statistical method which does not rely on identifying individual lines, and which is free from any systematic effects associated with line counting. In this paper we introduce a new technique based on the statistical properties of the transmitted flux. The method is a space-scale decomposition and as such retains spatial information. It allows us to locate specific structures in the Ly α forest, and assess their significance, as compared to a random distribution. The method is compared to a line counting/tpcf method, and we show that it is substantially more sensitive.

The organisation of this paper is as follows: in section 2 we describe the new analysis and carry out all necessary analytic calculations. In section 3 we use Monte-Carlo simulations to compare the new method with a tpcf analysis. We present our conclusions in section 4.

2 TECHNIQUE

We base our analysis on the null-hypothesis that any Ly α forest spectrum can be fairly well represented by a collection of individual absorption lines (Carswell et al. 1984; Kirkman & Tytler 1997; Lu et al. 1996; Hu et al. 1995) whose parameters are uncorrelated. Usually those lines are taken to be Voigt profiles and we shall adopt this although the exact shape of the profile is not relevant. We also need to adopt the functional form of the distribution of the absorption line parameters, $\eta(z, N, b)$, which we take from observations. We stress that we make *no* assumptions about what causes the absorption lines. Our analysis does not rely on identifying an absorption line with an individual, well-defined absorbing cloud. The composition of a spectrum of individual lines is purely descriptive. We simply use the null-hypothesis to predict integral properties of the absorption caused by the collection of lines.

The general idea of the new analysis then is to use those predictions to identify over- and underdense regions of absorption as a function of scale and position (space-scale decomposition) and to assess their statistical significance. This is implemented by using a matched filter technique; in order to obtain an estimate of the mean transmission we simply convolve a normalised spectrum (of N_p pixels) with a smoothing function of scale σ_s and repeat this process for all possible scales ($\sigma_s = 1, \dots, N_p$). When plotted in the (λ, σ_s) plane, this procedure results in the ‘transmission triangle’ of the spectrum. When using a top hat function as the smoothing function the base of the transmission triangle is the spectrum itself (the original spectrum smoothed by a top hat of width $\sigma_s = 1$ pixel) and the tip of the triangle is $1 - D_A$ (Oke & Korycansky 1982) (the original spectrum smoothed by a top hat of width $\sigma_s = N_p$ pixels). Since we are only interested in local fluctuations of the transmission around the mean, we then subtract out the mean as calculated on the basis of our null-hypothesis. Essentially, this removes the global redshift evolution of the optical depth. The statistical significance of any remaining residual fluctuations around zero are then assessed in terms of the expected rms as a function of wavelength and scale.

In the rest of this section we calculate the relevant quantities. The work presented here is developed from earlier calculations carried out by Zuo & Phinney (1993), Zuo (1993), and Zuo & Bond (1994) (but see also Press, Rybicki, & Schneider 1993). For completeness and clarity we reiterate some of their derivations here. When considering the expected mean transmission and its variance it is helpful to introduce the concept of transmission probability. The idea is to view a Ly α forest spectrum as a random stochastic process (Press, Rybicki, & Schneider 1993). Every point in the spectrum is a random variable, $e^{-\tau}$, drawn from the transmission probability density function $f_\lambda(e^{-\tau})$, also known as flux decrement distribution function (Rauch et al. 1997; Kim et al. 1997) or distribution of intensities (Jenkins & Ostriker 1991; Webb et al. 1992). In principle, we have a different probability density function at each wavelength such that e.g. the moments of f_λ are functions of wavelength. There is a small and subtle difference between the transmission probability density function and the distribution of pixel intensities of a spectrum. f_λ should in principle be measured by constructing the frequency distribution of pixel intensities at λ (and only at λ) of many different spectra. Although this is important to note we shall see later that at least the first and second moments of f_λ are only slowly varying functions of λ so that in many calculations we can approximate $e^{-\tau}$ as a stationary stochastic process.

2.1 The mean Ly α transmission

Given the distribution of absorption line parameters $\frac{dN}{dz dN db} = \eta(z, N, b)$, what is the mean transmission at a given wavelength? We can define an effective optical depth, τ_{eff} , as a function of observed wavelength, λ , by

$$e^{-\tau_{\text{eff}}(\lambda)} \equiv \langle e^{-\tau(\lambda)} \rangle. \quad (1)$$

In the following we will neglect any contribution to τ_{eff} from the classical Gunn-Peterson effect which is limited to $\tau_{\text{GP}} \lesssim 0.04$ (Webb et al. 1992). If the number of absorption lines per sight-line is Poisson distributed with a mean of $m = \int_0^\infty \int_0^\infty \int_{z_1}^{z_2} \eta(z, N, b) dz dN db$ then we have

$$e^{-\tau_{\text{eff}}} = \sum_{k=0}^{\infty} p(k; m) \langle e^{-\tau_s} \rangle^k, \quad (2)$$

where $p(k; m) = e^{-m} m^k / k!$ and

$$\langle e^{-\tau_s(\lambda)} \rangle = \int_0^\infty \int_0^\infty \int_{z_1}^{z_2} \frac{\eta(z, N, b)}{m} e^{-\tau_s(\lambda_z; N, b)} dz dN db. \quad (3)$$

$\tau_s(\lambda_z; N, b)$ is the profile of a single absorption line at z, N, b where $\lambda_z = \lambda/(1+z)$. After some algebra we find

$$\begin{aligned} \tau_{\text{eff}} = m(1 - \langle e^{-\tau_s} \rangle) &= \int \eta(1 - e^{-\tau_s(\lambda_z)}) dz dN db \\ &= \lambda \int_0^\infty \int_0^\infty \int_{\lambda_{z_2}}^{\lambda_{z_1}} \frac{\eta}{\lambda_z^2} (1 - e^{-\tau_s(\lambda_z)}) d\lambda_z dN db \end{aligned} \quad (4)$$

If we exclude strongly saturated and damped systems from our analysis then $\tau_s(\lambda_z)$ peaks sharply at $\lambda_z = \lambda_\alpha = 1215.67 \text{ \AA}$ so that

$$\tau_{\text{eff}} \simeq \frac{1 + z_{\text{abs}}}{\lambda_\alpha} \iint \eta(z_{\text{abs}}, N, b) \int_{\lambda_{z_2}}^{\lambda_{z_1}} (1 - e^{-\tau_s(\lambda_z)}) d\lambda_z dN db, \quad (5)$$

where $z_{\text{abs}} = \lambda/\lambda_\alpha - 1$. Usually, $z_1 = \lambda_\beta/\lambda_\alpha(1 + z_{\text{em}}) - 1$, where $\lambda_\beta = 1025.72 \text{ \AA}$, and in the absence of a proximity effect $z_2 = z_{\text{em}}$. For λ close to $\lambda_\alpha(1 + z_{\text{em}})$, there are fewer than average absorption lines longward of λ . This produces an ‘edge effect’, superimposed on the well-known proximity effect (Weymann, Carswell, & Smith 1981; Cooke, Espey, & Carswell 1997). Similarly, there will be a reverse edge effect for λ close to $\lambda_\beta(1 + z_{\text{em}})$ because of the additional absorption by Ly β lines. If λ falls well away from these limits then we can extend the upper and lower integration limits in (5) to ∞ and 0 respectively because if λ_z and λ_α are sufficiently far apart $1 - e^{-\tau_s}$ is zero. Thus we have

$$\tau_{\text{eff}} \simeq \frac{1 + z_{\text{abs}}}{\lambda_\alpha} \int \eta(z_{\text{abs}}, N, b) W(N, b) dN db. \quad (6)$$

Observationally η is found to be of the form $\eta(z, N, b) = (1+z)^\gamma F(N, b)$ (Kim et al. 1997; Lu et al. 1996; Bechtold 1994; Williger et al. 1994; Bahcall et al. 1993). We therefore arrive at

$$\tau_{\text{eff}} = B(1 + z_{\text{abs}})^{\gamma+1} = B \left(\frac{\lambda}{\lambda_\alpha} \right)^{\gamma+1}, \quad (7)$$

where

$$B = \frac{1}{\lambda_\alpha} \int_0^\infty \int_0^\infty F(N, b) W(N, b) dN db. \quad (8)$$

In practice, we compute B directly from the data for reasons described in section 3. Thus we have

$$\langle e^{-\tau} \rangle = e^{-B \left(\frac{\lambda}{\lambda_\alpha} \right)^{\gamma+1}}. \quad (9)$$

2.2 The auto-covariance

The auto-covariance function of the transmission is given by

$$\begin{aligned} \gamma_{e^{-\tau}}(\lambda, \lambda') &= \left\langle \left(e^{-\tau(\lambda)} - \langle e^{-\tau(\lambda)} \rangle \right) \left(e^{-\tau(\lambda')} - \langle e^{-\tau(\lambda')} \rangle \right) \right\rangle \\ &= \langle e^{-\tau(\lambda)} e^{-\tau(\lambda')} \rangle - e^{-\tau_{\text{eff}}(\lambda)} e^{-\tau_{\text{eff}}(\lambda')} \\ &\equiv e^{-\Pi(\lambda, \lambda')} - e^{-\tau_{\text{eff}}(\lambda)} e^{-\tau_{\text{eff}}(\lambda')}. \end{aligned} \quad (10)$$

Following the same calculations as in the previous section, we find

$$\Pi(\lambda, \lambda') = \int \eta(z, N, b) (1 - e^{-\tau_s(\lambda)} e^{-\tau_s(\lambda')}) dz dN db. \quad (11)$$

Let us consider the variance of the transmission given by

$$\sigma_{e^{-\tau}}^2 = \gamma_{e^{-\tau}}(\lambda, \lambda). \quad (12)$$

Since $\tau_s(N) \propto N$, we have $2\tau_s(N) = \tau_s(2N)$ and thus we get similarly to equation (7)

$$\Pi(\lambda, \lambda) = \tilde{B}(1+z)^{\gamma+1}, \quad (13)$$

where

$$\tilde{B} = \frac{1}{\lambda_\alpha} \int_0^\infty \int_0^\infty F(N, b) W(2N, b) dN db. \quad (14)$$

Observations have shown that the distribution of column densities can be fairly well represented by a power law, $F(N, b) = N^{-\beta} f(b)$ (Carswell et al. 1984) with $\beta \approx 1.5$ (Kim et al. 1997; Kirkman & Tytler 1997; Lu et al. 1996; Hu et al. 1995). A finite number of absorption lines per line of sight implies that the power law must break off at the low N end at some N_{low} . We also expect a break at the high N end at some N_{hi} . Thus we have

$$\tilde{B} = \frac{2^{\beta-1}}{\lambda_\alpha} \int_0^\infty \int_{2N_{\text{low}}}^{2N_{\text{hi}}} F(N, b) W(N, b) dN db. \quad (15)$$

We know that the power law is a good approximation for the range $12 \lesssim \log N/\text{cm}^{-2} \lesssim 22$ (Hu et al. 1995; Petitjean et al. 1993), so that N_{low} and N_{hi} are in the linear and square-root regimes of the curve of growth respectively. Under this assumption it is straightforward to show that \tilde{B} can be well approximated by $2^{\beta-1}B$ for $\beta \lesssim 1.8$, this being the exact result (for all β) if there are no breaks in the power law. Therefore we finally arrive at

$$\sigma_{e^{-\tau}}^2 = e^{-2^{\beta-1}B(1+z)^{\gamma+1}} - e^{-2B(1+z)^{\gamma+1}}. \quad (16)$$

2.3 Instrumental effects

So far we have not considered any instrumental effects. There are two classes of such effects: finite spectral resolution and various sources of noise.

2.3.1 Finite resolution

A new stochastic variable X is produced by convolving $e^{-\tau}$ with a line spread function (LSF) L :

$$X(\lambda) = \int_{-\infty}^{\infty} e^{-\tau(\lambda')} L(\lambda - \lambda') d\lambda' \quad (17)$$

For the mean of X we get

$$\langle X \rangle = \int_{-\infty}^{\infty} \langle e^{-\tau(\lambda')} \rangle L(\lambda - \lambda') d\lambda'. \quad (18)$$

Although it has been stressed that the mean and the variance of $e^{-\tau}$ are functions of λ we will now approximate $e^{-\tau}$ as a *stationary* stochastic process because both the mean and the variance are smooth, slowly varying functions of λ . Lu & Zuo (1994) have shown this approximation to be valid. Thus we have

$$\langle X \rangle(\lambda) \simeq e^{-\tau_{\text{eff}}(\lambda)} \quad (19)$$

since the LSF is normalised to unity. As is intuitively clear, the convolution does not change the mean transmission.

The auto-covariance function of X is given by

$$\begin{aligned} \gamma_X(\lambda_1, \lambda_2) &= \langle (X(\lambda_1) - \langle X \rangle(\lambda_1)) (X(\lambda_2) - \langle X \rangle(\lambda_2)) \rangle \\ &= \iint_{-\infty}^{+\infty} L(\lambda_1 - \lambda'_1) L(\lambda_2 - \lambda'_2) \gamma_{e^{-\tau}}(\lambda'_1, \lambda'_2) d\lambda'_1 d\lambda'_2. \end{aligned} \quad (20)$$

Since we consider $e^{-\tau}$ to be a *stationary* process, $\gamma_{e^{-\tau}}$ depends only on $u' = \lambda'_2 - \lambda'_1$ and γ_X depends only on $u = \lambda_2 - \lambda_1$ (Jenkins & Watts 1968). Usually, the LSF can be well approximated as a Gaussian. After some algebra we get

$$\gamma_X(u) = \frac{1}{\sqrt{2\pi}\sigma'_{\text{LSF}}} \int_{-\infty}^{\infty} \gamma_{e^{-\tau}}(u') \exp\left(-\frac{(u-u')^2}{2\sigma'^2_{\text{LSF}}}\right) du', \quad (21)$$

where $\sigma'_{\text{LSF}} = \sqrt{2}\sigma_{\text{LSF}}$.

2.3.2 Noise

The noise in optical spectra is mainly due to photon counting statistics, detector read-out noise, dark current, sky subtraction, and cosmic rays. As the Poisson statistics of the absorption lines are expected to dominate the variance we have not attempted to model the noise characteristics in great detail. We rather approximate the cumulative effect of all the noise components mentioned above to be Gaussian. Therefore, we define the stochastic variable Y by

$$Y(\lambda) = X(\lambda) + n(X(\lambda)), \quad (22)$$

where n is a random variable drawn from a Gaussian with mean zero and variance $\sigma_n^2(X) = X(c_1 - c_2) + c_2$. The constants c_1 and c_2 characterise the photon counting statistics and the sky subtraction plus detector noise ($c_1 > c_2$). For the mean of Y we have

$$\langle Y \rangle = \langle X \rangle + \langle n \rangle = \langle X \rangle = \langle e^{-\tau} \rangle \quad (23)$$

and the covariance is given by

$$\gamma_Y(\lambda_1, \lambda_2) = \gamma_X(\lambda_1, \lambda_2) + \gamma_{Xn}(\lambda_1, \lambda_2) + \gamma_{Xn}(\lambda_2, \lambda_1) + \gamma_n(\lambda_1, \lambda_2). \quad (24)$$

γ_{Xn} denotes the *cross-covariance* function of X and n . Although X and n are not *independent* they are, by construction, *uncorrelated*, so that $\gamma_{Xn} = 0$. Zuo & Bond (1994) showed that the originally uncorrelated photon noise in different wavelength bins remains uncorrelated after passing through a spectrograph of finite resolution. Therefore $\gamma_n(u)$ must be discontinuous at $u = 0$:

$$\gamma_n(u) = \begin{cases} 0 & u > 0 \\ \int f_X(x) \sigma_n^2(x) dx & u = 0 \end{cases} \quad (25)$$

where $f_X(x)$ denotes the pdf of X . The integral reduces to $\sigma_n^2(\langle X \rangle)$. Thus

$$\begin{aligned} \sigma_Y^2 &= \sigma_X^2 + \sigma_n^2(\langle X \rangle) \\ \gamma_Y(u) &= \gamma_X(u) \quad u > 0. \end{aligned} \quad (26)$$

2.4 Filter matching

In order to develop a method for detecting structures of arbitrary scale, we proceed by convolving the spectrum with a smoothing function of smoothing scale σ_s . The convolution filters out all power on scales smaller than σ_s . By changing the width of the smoothing function we can match the filter width to the scale of any feature and thus maximise its signal. In practice, we perform the convolution successively at all possible smoothing scales. At the largest possible scale ($\sigma_{s,\max}$ = number of pixels in the spectrum) the entire spectrum is compressed into a single number whereas on the smallest scale ($\sigma_{s,\min} = 1$ pixel) the spectrum remains essentially unchanged. These two extremes correspond to the tip and the base of the triangle which forms when the successive convolutions of the spectrum are plotted in the (λ, σ_s) plane. In principle, there are many choices for the specific form of the smoothing function but for simplicity we will use a Gaussian, thus constructing a new stochastic variable G :

$$G(\lambda, \sigma_s) = \frac{1}{\sqrt{2\pi} \sigma_s} \int_{-\infty}^{\infty} Y(\lambda') \exp\left(-\frac{(\lambda - \lambda')^2}{2\sigma_s^2}\right) d\lambda'. \quad (27)$$

As in section 2.3.1 we have

$$\langle G \rangle(\lambda) \simeq e^{-\tau_{\text{eff}}(\lambda)} = e^{-B(\frac{\lambda}{\lambda_\alpha})^{\gamma+1}}. \quad (28)$$

Note that the use of a top hat function would yield a variable akin to $1 - D_A$ (and the same result as equation (28)), where D_A is the flux deficit parameter (Oke & Korycansky 1982). The observations are consistent with this result (Press, Rybicki, & Schneider 1993; Zuo & Lu 1993; but see also Bi & Davidsen 1997). Similar to equation (21) we find

$$\begin{aligned} \gamma_G(u) &= \frac{1}{\sqrt{2\pi} \sigma'_s} \int_{-\infty}^{\infty} \gamma_Y(u') \exp\left(-\frac{(u - u')^2}{2\sigma_s'^2}\right) du' \\ &= \frac{\sigma_n^2(e^{-\tau_{\text{eff}}})}{\sqrt{2\pi} \sigma'_s / ps} e^{-\frac{u^2}{2\sigma_s'^2}} + \frac{1}{\sqrt{2\pi} \sqrt{\sigma_s'^2 + \sigma_{\text{LSF}}'^2}} \int_{-\infty}^{\infty} \gamma_{e^{-\tau}}(u'') \exp\left(-\frac{(u - u'')^2}{2(\sigma_s'^2 + \sigma_{\text{LSF}}'^2)}\right) du'' \end{aligned} \quad (29)$$

where ps denotes the pixel size in \AA . To proceed we need to consider the auto-covariance function of a ‘perfect’ spectrum, $\gamma_{e^{-\tau}}$, in more detail. In principle, it can be calculated from equation (11) as was done by Zuo & Bond (1994) for a single Doppler parameter rather than a distribution of b values. The result is a rather unwieldy numerical integral. Here we can take a different approach. As expected, we can see from equation (29) that the quantity that we are interested in, $\sigma_G^2 = \gamma_G(0)$, does *not* depend on the exact shape of $\gamma_{e^{-\tau}}$ but rather on the convolution of $\gamma_{e^{-\tau}}$ with a Gaussian. We may therefore hope to

be able to use a simpler analytic approximation for $\gamma_{e^{-\tau}}$ since all systematic differences will be somewhat ‘washed out’ by the convolution. Ultimately, this procedure must be justified by its success. We shall return to this point when we compare the results of this section to simulations. The most obvious (because simplest) approximation for $\gamma_{e^{-\tau}}$ is a Gaussian, especially when considering that unsaturated Voigt profiles are very nearly Gaussian:

$$\gamma_{e^{-\tau}}(u) \simeq \sigma_{e^{-\tau}}^2 e^{-\frac{u^2}{2q^2}}. \quad (30)$$

Since we are operating in wavelength space rather than in velocity space the width, q , must be a function of wavelength, because an absorption line with a given Doppler parameter will be wider in wavelength space at higher redshifts than at lower redshifts. This is of course just another reflection of the fact that $e^{-\tau}$ is not a stationary process. But again, q will vary only slowly with wavelength (approximately linearly) so that the stationary approximation is valid. Using this approximation we find

$$\sigma_G^2(\lambda, \sigma_s) = \frac{\sigma_n^2(e^{-\tau_{\text{eff}}(\lambda)})}{2\sqrt{\pi} \sigma_s / ps} + \frac{\sigma_{e^{-\tau}}^2(\lambda)}{\sqrt{2 \frac{\sigma_s^2 + \sigma_{\text{SFE}}^2}{q^2(\lambda)} + 1}}. \quad (31)$$

Equations (28) and (31) are the final result of this section.

3 SIMULATIONS

The motivation for simulations of Ly α forest spectra in this work is threefold. First of all we need to determine the parameters B and q . The normalisation B could be calculated numerically from equation (8). However, it is clear that for real data small inaccuracies in the zeroth and first order of the continuum fit will cause an artificial offset of the measured mean transmission from the calculated one. In anticipation of this problem we choose to determine B directly from the data. Since equation (30) is only an approximation we cannot *a priori* calculate a precise value for q . We therefore have to measure it from simulations. Secondly, we would like to check the validity of equations (28) and (31) by comparing the calculations with an analysis of simulated spectra. Thirdly, we would like to compare the sensitivity of the new analysis to the presence of non-random structures to that of the traditional line counting technique. In order to cater for this third need, we employed a more sophisticated method than simply randomly drawing the parameters of absorption lines from a given distribution $\eta(z, N, b)$. Instead we distribute absorbers in a cosmological volume and take lines of sight through that volume. This provides the flexibility of introducing specific types of clustering models. We assume absorbers to be spherical and prescribe a column density – impact parameter relationship of the form $N(r) = N_0(r/r_0)^{-a}$ which has been observed at low redshift where galaxies are unambiguously associated with Ly α absorbers (Chen et al. 1998; Lanzetta, Webb, & Barcons 1996; Lanzetta et al. 1995; but see also Bowen, Blades, & Pettini 1996). This procedure simply ensures that the column density distribution of the absorption lines will be of the form $N^{-\beta}$ with $\beta = 2/a + 1$. We draw Doppler parameters from a truncated Gaussian. We choose to keep the comoving number density of absorbers constant and thus ascribe their redshift evolution solely to the evolution of their absorption cross-section. This requires a redshift dependence of r_0

$$r_0(z) = r_0(\hat{z}) \frac{(1 + 2q_0 z)^{\frac{1}{4}} (1 + z)^{\frac{\gamma-1}{2}}}{(1 + q_0)^{\frac{1}{4}} (1 + \hat{z})^{\frac{\gamma-1}{2}}} \quad (32)$$

where we take the normalisation $r_0(\hat{z}) = 1 h^{-1}$ Mpc at $N_0 = 10^{12} \text{ cm}^{-2}$ from Lanzetta et al. (1995) at $\hat{z} = 0.5$.

3.1 B and q from simulations

In order to compare equations (28) and (31) with simulations we have produced a set of 1000 spectra in the manner described in the previous section with randomly distributed absorbers. The spectra are convolved with a line spread function and noise is added according to equation (22). The parameters of the simulation are listed in Table 1 (S1). For each spectrum we constructed its transmission triangle using a Gaussian smoothing function. From this set of 1000 triangles we produced the mean and rms transmission triangles which are shown in Figures (1) and (2). Before we can go on to compare these results with equations (28) and (31) we must determine the values of the two parameters B and q . We fix the normalisation B at the tip of the mean transmission triangle by requiring

$$\langle G \rangle(\sigma_{s,\text{max}}, \lambda_c) = e^{-B(\frac{\lambda_c}{\lambda_\alpha})^{\gamma+1}}, \quad (33)$$

where $\sigma_{s,\text{max}}$ denotes the biggest possible smoothing scale and λ_c is the central wavelength of the region under consideration. Having stipulated equation (30) we measure q (at λ_c) from the simulations by performing a single parameter χ^2 fit of the function

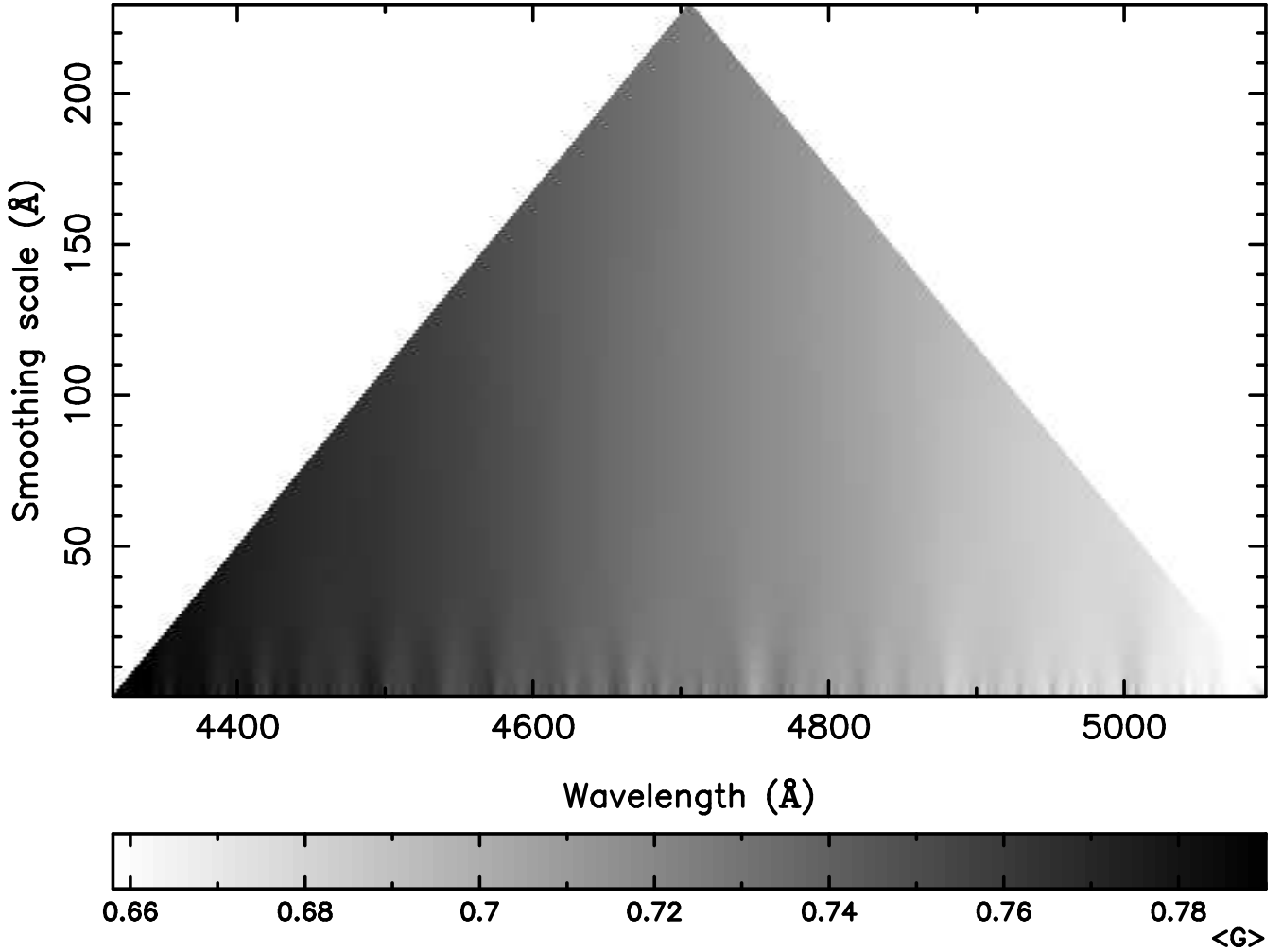


Figure 1. Mean transmission triangle produced from 1000 simulated spectra.

Table 1. Parameters of simulations.

	γ	β	n_0 ($h^3 \text{ Mpc}^{-3}$)	μ_b (km s^{-1})	σ_b (km s^{-1})	b_{cut} (km s^{-1})	S/N	FWHM_{LSF} (\AA)
S1	2.5	1.5	0.01	30	8	18	20	2
S2	2.5	1.7	0.01	30	8	18	20	2
S3	2.7	1.5	0.01	30	8	18	20	2
S4	2.5	1.5	0.015	30	8	18	20	2
S5	2.5	1.5	0.01	50	8	38	20	2
S6	2.5	1.5	0.01	30	16	18	20	2
S7	2.5	1.5	0.01	30	8	18	20	0.5
S8	2.5	1.5	0.01	30	8	18	5	2

n_0 is the comoving number density of absorbers (normalisation of $\eta(z, N, b)$), μ_b , σ_b , and b_{cut} are the mode, width, and lower cut-off of the Doppler parameter distribution respectively. For models S1 and S7 we created 1000 spectra, in all other cases we simulated 100 spectra. For all spectra $\langle z \rangle = 2.87$.

$$\gamma_Y(u) = \begin{cases} \sigma_n^2(e^{-\tau_{\text{eff}}(\lambda_c)} + \frac{\sigma_{e^{-\tau}}^2(\lambda_c)}{\sqrt{2\frac{\sigma_{\text{LSF}}^2}{q^2} + 1}} & u = 0 \\ \frac{\sigma_{e^{-\tau}}^2(\lambda_c)}{\sqrt{2\frac{\sigma_{\text{LSF}}^2}{q^2} + 1}} \exp\left(\frac{-u^2}{2(2\sigma_{\text{LSF}}^2 + q^2)}\right) & u > 0 \end{cases} \quad (34)$$

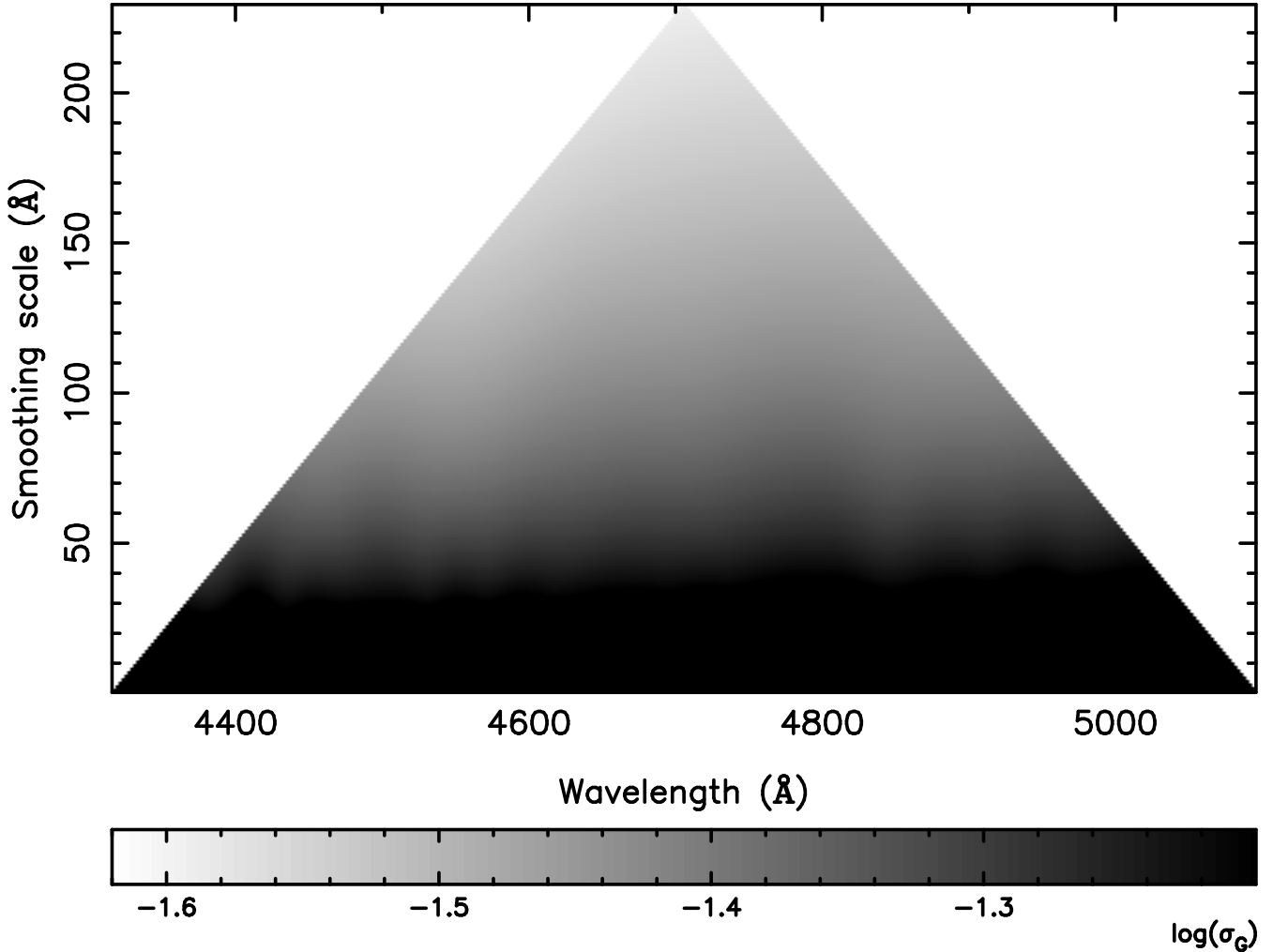


Figure 2. Rms transmission triangle produced from 1000 simulated spectra.

to the mean auto-covariance function of the 1000 simulated spectra. Since equation (30) (and hence equation (34)) is an approximation we do not *a priori* expect a statistically acceptable fit. Nevertheless, in practice this procedure provides a reliable estimate of q because both the shape (width) *and* normalisation of γ_Y are sensitive to q . Figure (3) shows the measured mean auto-covariance function of S1 and its fit. The same is also plotted for two other sets of spectra (c.f. Table 1), S7 (same model as S1 but the spectra are of higher resolution) and S5 (larger mode of the Doppler parameter distribution). It is evident that a Gaussian does not adequately represent the auto-covariance functions; a Gaussian has too much power on small scales and too little power on larger scales. Indeed, each fit produces an unacceptably large χ^2 , although we point out that in any case a somewhat larger than usual χ^2 must be anticipated because of the non-Gaussian and correlated nature of the measurement errors of γ_Y . However, we recall that we are mostly interested in the typical width and strength of the correlation rather than its exact shape. Since both sets of spectra S1 and S7 should yield the same value for q , the purpose of set S7 was to check whether the above method of determining q is robust and to provide an estimate of the true error in q as opposed to the formal error as calculated from the χ^2 fit. As expected, q is of the order of the mode Doppler parameter, μ_b , for a range of sensible values for μ_b , as seen from S5. In fact, q is seen to vary almost linearly with μ_b , which justifies $q(\lambda) = q(\lambda_c)\lambda/\lambda_c$. We have also investigated the behaviour of q as a function of the other model parameters and have found, as expected, that q is only sensitive to the parameters of the Doppler parameter distribution, μ_b and σ_b , and of the column density distribution, β . It is insensitive to the redshift evolution, overall normalisation, and the quality of spectra since the q values measured from models S3, S4, S7, and S8 are all comparable. We conclude that the error in estimating q is dominated by the errors in μ_b , σ_b and β .

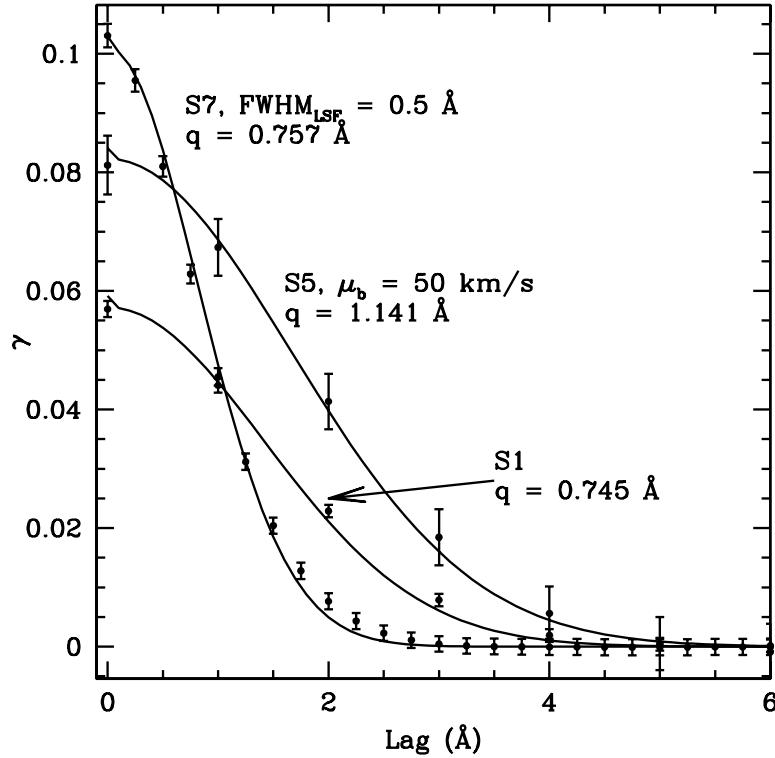


Figure 3. Auto-covariance functions of different models as indicated and best fits (solid lines). For clarity, all errorbars have been exaggerated by a factor of 10.

3.2 Comparison of analytical to numerical results

With the values of B and q thus determined we can now directly compare the results from the simulations with equations (28) and (31). Figures (4) and (5a) show cross sections of the mean and rms transmission triangles of S1 as functions of wavelength at smoothing scale $\text{FWHM}_s = 3.2 \text{ \AA}$. Figure (5b) shows a cross section through the rms transmission triangle as a function of smoothing scale at $z = 2.87$. The dashed lines show the calculations. Using the covariance matrix implied by equation (34), a χ^2 test performed on the base of the mean transmission triangle yields $P(> \chi^2) = 0.12$ and thus the model agrees very well with the simulations. For the rms the agreement is not quite as good. We find that for very large smoothing scales ($\text{FWHM}_s > 100 \text{ \AA}$) the model underestimates the rms by ~ 4 per cent. For smaller (and more relevant) scales the model fares progressively better.

We have repeated this exercise for all sets of simulations listed in Table 1 and have always found the same good agreement. In addition, we have repeated the calculations in section (2.4) and the analysis of the simulated data for the case of a top hat smoothing function and these also agree very well. Thus we conclude that the errors in determining any fluctuations of the Ly α absorption around its expected mean and in estimating their significance will be dominated by the uncertainties in the assumed values of the parameters β , μ_b , σ_b and to lesser extent γ and the overall normalisation. Any errors made in any of the approximations of the previous sections are small compared to these uncertainties.

3.3 Sensitivity

With all the calculations and parameter values in place we can now answer the questions: ‘How statistically significant is an enhancement of the local absorption line number density over the mean line number density at redshift z by a factor of δn on the scale of $x h^{-1} \text{ Mpc}$?’ and ‘At what redshift is an overdensity of δn on the scale of $x h^{-1} \text{ Mpc}$ most significant?’ To address these questions we plot the quantity

$$\frac{e^{-\delta n \tau_{\text{eff}}} - e^{-\tau_{\text{eff}}}}{\sigma_G}$$

in Figures (6a) and (b) as a function of δn and z respectively for a scale of $5 h^{-1}$ proper Mpc (FWHM of smoothing Gaussian), assuming the parameters of S1. From Figure (6a) we see that for a given redshift we can expect a maximum signal which

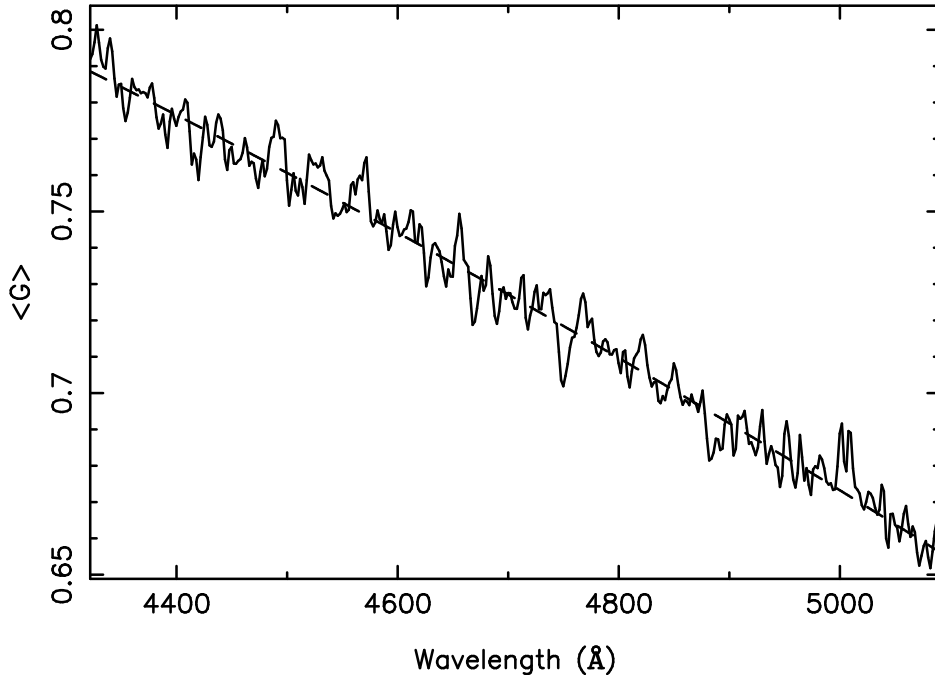


Figure 4. Cross section of the mean transmission triangle (c.f. Figure 1) at $\text{FWHM}_s = 3.2 \text{ \AA}$. The dashed line shows the prediction of equation (28).

cannot be exceeded. This is due to saturation as the number density of absorption lines increases rapidly towards higher redshift. Figure (6b) tells us that for a given level of overdensity there is an optimum redshift at which this level of overdensity will produce a maximum signal.

At this point it is necessary to comment on the exact significance of, e.g., a ‘ 3σ event’. For small smoothing scales the pdf of G is inherently non-Gaussian such that we expect the probability of G lying within 3σ of the mean to be smaller than 0.9973. In fact the pdf is skewed such that the probability of a $+3\sigma$ event (a void) is lower than the probability of a -3σ event (a cluster). At larger smoothing scales the Central Limit Theorem guarantees Gaussianity. Thus a 3σ event at large smoothing scales is statistically more significant than a similar event at small smoothing scales. This additional complication must be kept in mind.

3.4 Comparison to TPCF

Groups of QSOs that are closely spaced in the plane of the sky can be used to map out the large-scale 3-dimensional structure of the intervening absorbing gas by identifying absorption features that are approximately coincident in redshift space in two or more spectra. One of the advantages of the analysis presented here is that it can easily be applied to the spectra of such groups: the transmission triangles of the different spectra are simply averaged where they overlap. For sight-line separations of several arcminutes, different lines of sight will not intersect the same absorber, so that according to our null-hypothesis of an unclustered Ly α forest different lines of sight are uncorrelated. Therefore the variance of a mean transmission triangle (averaged over multiple lines of sight) at (λ, σ_s) is simply given by $\sigma_G^2(\lambda, \sigma_s)$ divided by the number of triangles overlapping at (λ, σ_s) . Thus the signal of any structure extending across several lines of sight will be enhanced.

In order to compare our analysis directly to a ‘traditional’ two-point correlation function analysis we have simulated spectra of a close group of QSOs where the absorbers are clustered. In view of the modern, large hydrodynamic simulations of structure formation which reproduce many of the observed properties of the Ly α forest, the simulations presented here must be understood in the sense of a toy model. The advantage of our simulation is the flexibility to model different clustering characteristics, thus enabling us to test our method comprehensively. It is not important for these particular clustering models to describe reality accurately since our aim is to compare the relative sensitivity of a two-point correlation function analysis and the technique we have developed here. The validity of this test is unlikely to depend strongly on the type of clustering. We have explored two clustering scenarios:

1) Absorbers are clustered according to the gravitational quasi-equilibrium distribution (GQED) function (Saslaw & Hamilton 1984). We implement this scenario by following an approach first developed by Neyman & Scott (1952) and described

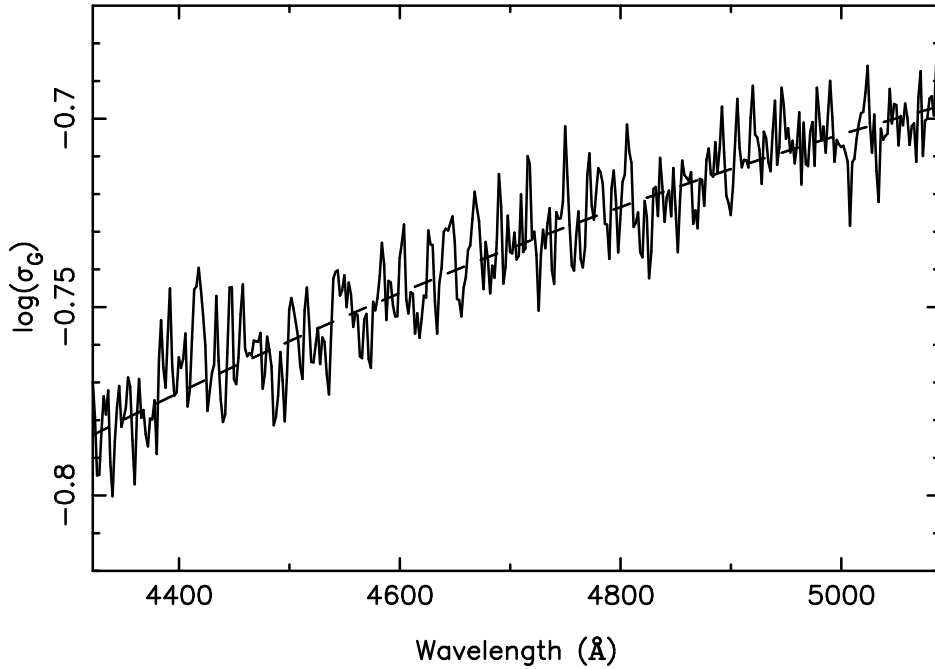


Figure 5. (a) Cross section of the rms transmission triangle (c.f. Figure 2) at $\text{FWHM}_g = 3.2 \text{ \AA}$. The dashed line shows the prediction of equation (31).

by Sheth & Saslaw (1994): we distribute clusters of absorbers randomly in a cosmological volume and draw the number of absorbers of a given cluster from the distribution (Saslaw 1989)

$$h(N) = \begin{cases} b & N = 0 \\ \frac{N^{N-1}}{N!} (1-b)b^{N-1} e^{-Nb} & N > 0. \end{cases} \quad (35)$$

b is the only parameter of the model and is defined as the ratio of potential and kinetic energies of the cluster ($0 \leq b \leq 1$). It is related to the two-point correlation function by (Saslaw & Hamilton 1984)

$$b \equiv -\frac{W}{2K} = \frac{2\pi Gm^2 n}{3kT} \int_0^\infty \xi(r) dr, \quad (36)$$

where T and m are the temperature and mass of the cluster, n is the average number density and k and G have their usual meanings. We choose $b = 0.3$ (Sheth & Saslaw (1994) estimate for galaxies $b_0 \approx 0.75$) and members of a cluster have a velocity dispersion of 500 km s^{-1} . We assume clusters to be spherical and distribute absorbers within a cluster according to a King profile (King 1966).

2) Absorbers form ‘walls’. Considering the connection of the Ly α forest with galaxies at low redshift and the repeated findings of independent groups that galaxies form sheet- and wall-like structures (Broadhurst et al. 1990; Ettori, Guzzo, & Tarengi 1997; Einasto et al. 1997; Connolly et al. 1997; Di Nella et al. 1996) it is conceivable that such structures may also be found in the Ly α forest. In addition, at high redshift several hydrodynamic simulations have shown that the absorbing gas forms filaments, sheets and wall-like structures (Cen et al. 1994; Miralda-Escudé et al. 1996; Cen & Simcoe 1997; Hernquist et al. 1996; Zhang, Anninos, & Norman 1995; Petitjean, Mückel, & Kates 1995; Mückel et al. 1996; Riediger, Petitjean, & Mückel 1998; Wadsley & Bond 1997; Bond & Wadsley 1998), although these structures are of a smaller scale than we are interested in. In any case, we have included this model where walls of absorber overdensities extend across several lines of sight in order to demonstrate the better sensitivity of our analysis compared to a conventional *cross*-correlation analysis of fitted absorption lines.

For both scenarios we have computed 100 sets of simulated spectra of a close group of four QSOs using the parameters of S1.

Figure (7) shows the result of our new analysis for the case of GQED clustering. For all spectra we have computed their transmission triangles, subtracted the mean given by equation (28) and divided by the rms given by the square-root of equation (31). We shall refer to the result as ‘reduced’ transmission triangles. In the reduced triangles all residual fluctuations are given in terms of their statistical significance rather than their absolute magnitude. In panel (a) of Figure (7) we plot the histogram of the minimum values (maximally significant overdense absorption) measured in these reduced transmission

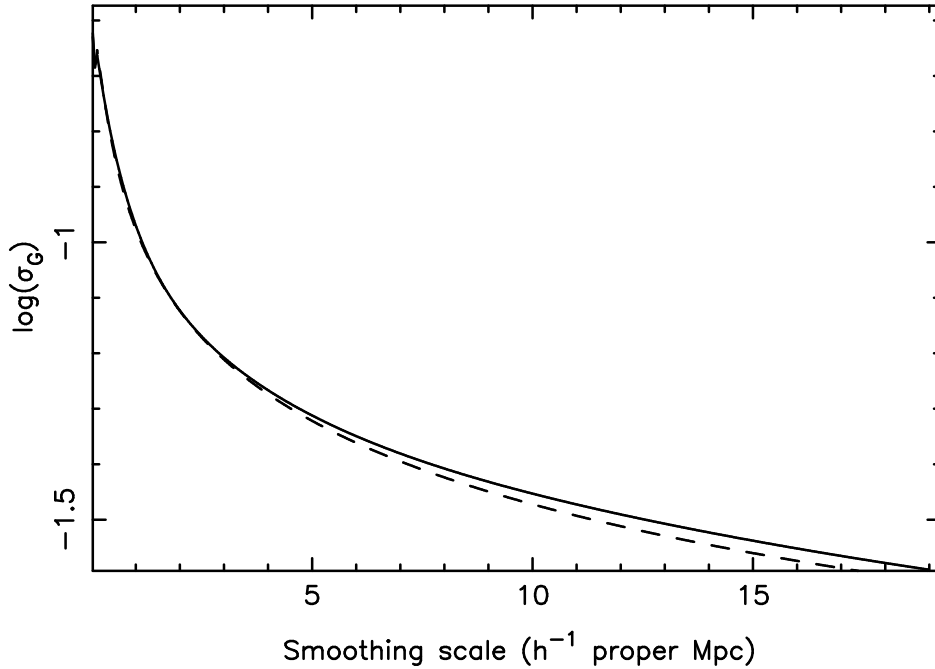


Figure 5 – *continued* (b) Cross section of the rms transmission triangle (c.f. Figure 2) at $z = 2.87$. The dashed line shows the prediction of equation (31).

triangles of the individual spectra. The distribution peaks at -3.6σ but in a significant fraction of cases (~ 40 per cent) we have a greater than 4σ detection. Panels (b) and (c) show that these detections are not spurious but actually arise from the clusters. In panel (b) we plot the distribution of scales (FWHM of smoothing Gaussian) at which the minima of panel (a) are detected. Clearly we recover the correct velocity dispersion of the clusters. We loosely define the ‘strongest’ cluster in a spectrum as the cluster with the highest total column density and plot in panel (c) the histogram of differences in velocity space between the strongest clusters and the detected minima, Δ . Although there is clearly a peak at 0 km s^{-1} of the correct width, there are a large number of cases where the detected minima do not coincide with the strongest clusters. However, these mismatches do *not all* indicate spurious detections. Rather, they are mostly due to our definition of the strongest cluster, since it does not guarantee that the strongest cluster will produce the maximum absorption.

We now compare the results above with a two-point correlation function (tpcf) analysis. We compute both ‘real’ and ‘observed’ tpcfs from two separate lists of absorption lines. A ‘real’ list is derived from the input line list used to create the spectrum by simply applying an equivalent width detection threshold. To mimic blending due to instrumental resolution we generate an ‘observed’ line list from the input line list by blending all lines that lie within one FWHM_{LSF} of each other into a single line and imposing an equivalent width detection limit. The position of the blended line is taken as the equivalent width weighted average of its components. We estimate the 3σ equivalent width detection limit in our simulated data to be 0.26 \AA . The two-point correlation function is calculated as

$$\xi(\Delta v) = \frac{N_{\text{obs}}(\Delta v)}{N_{\text{exp}}(\Delta v)} - 1, \quad (37)$$

where N_{obs} and N_{exp} are the observed and expected number of pairs at separation Δv . We account for the evolution of the mean line number density in the calculation of N_{exp} . The individual line correlation functions of a set of four spectra are averaged to increase the signal to noise ratio.

In panel (a) of Figure (8) we show the distribution of the maximally significant values detected in the averaged ‘observed’ (solid line) and ‘real’ (dotted line) two-point correlation functions. For an underlying clustered set of absorption lines, these distributions will be slightly sensitive to the bin size chosen in computing the tpcfs. To some extent this reflects one of the difficulties with the tpcf; one must chose *a priori* a bin size, without prior knowledge as to what an ‘optimal’ size might be. In practice, observers often chose the smallest convenient size which is larger than the instrumental resolution. We have done similarly in this experiment and have chosen 120 km s^{-1} .

The solid histogram in panel (a) peaks narrowly at 1.8σ . Only 3 per cent of the detections are $> 3\sigma$. Panel (b) shows the correlation scales at which the maxima are detected and we see that at least 50 per cent of the detections are spurious. The dotted histograms show the results for the ‘real’ tpcfs: significant detections (a) at the right scale (b). However, a comparison

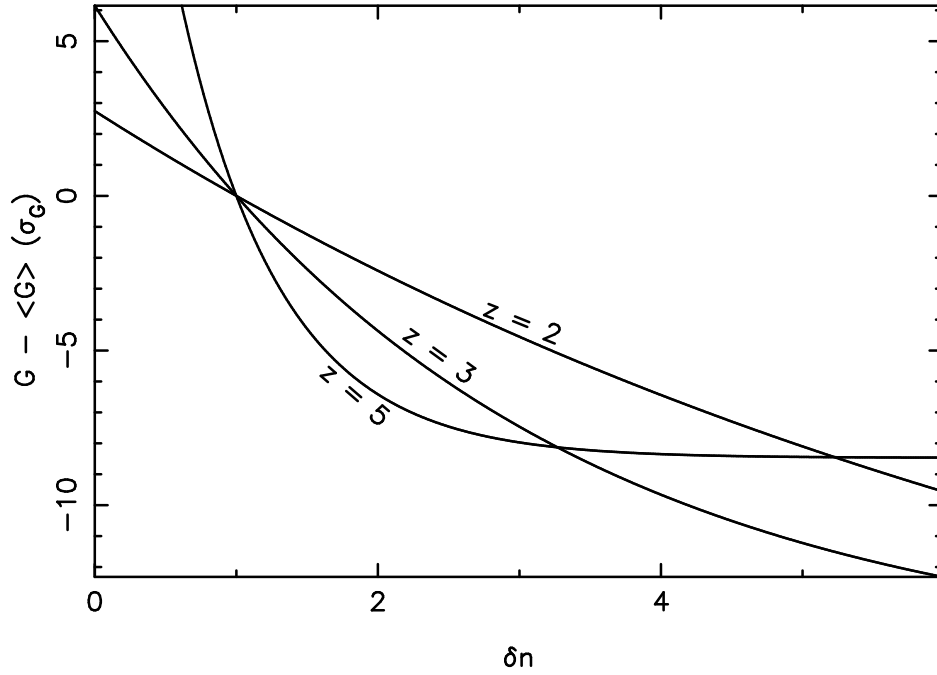


Figure 6. (a) Expected signal in units of σ_G of an overdensity of absorption lines of scale $5 h^{-1}$ proper Mpc (FWHM of smoothing Gaussian) at redshifts 2, 3, and 5.

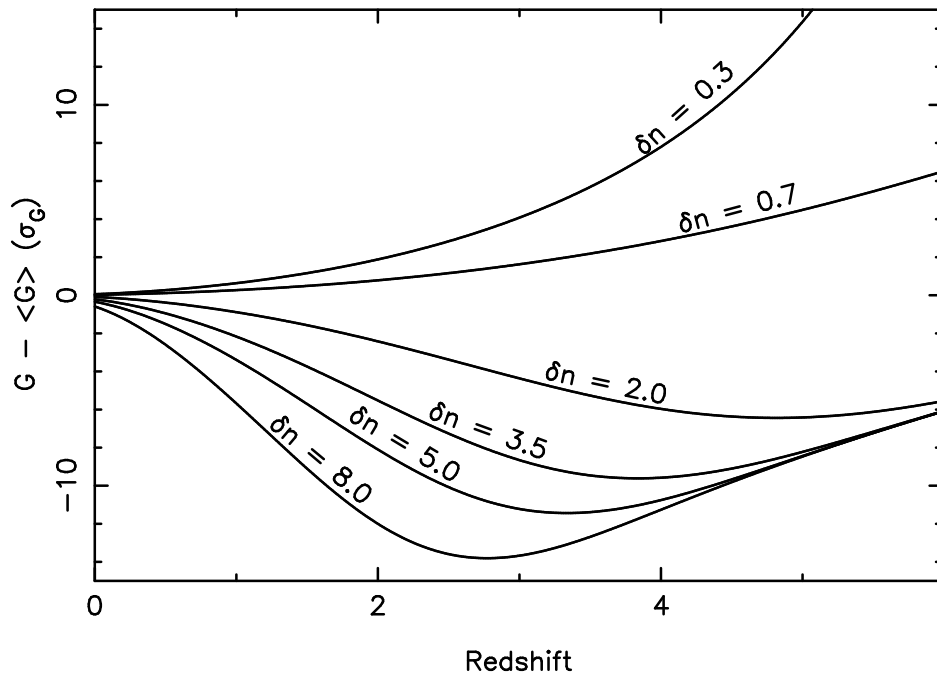


Figure 6 – continued (b) Same as (a) as a function of redshift for the indicated overdensities.

with panel (a) of Figure (7) shows that a tpcf analysis, even with *infinite* resolution (but finite S/N) and a *perfect* line fitting algorithm, does only marginally better in uncovering the presence of clustering than our new analysis using intermediate resolution.

Figure (9) shows the results for the case of a ‘wall’ of absorbers which is simulated by multiplying the redshift distribution of absorbers with a top hat function. The simulated wall is located at $z = 2.78$, it is $5 h^{-1}$ Mpc thick and is overdense by a factor of $\delta n = 2$. As described above we have averaged the individual transmission triangles of each set of four spectra. The

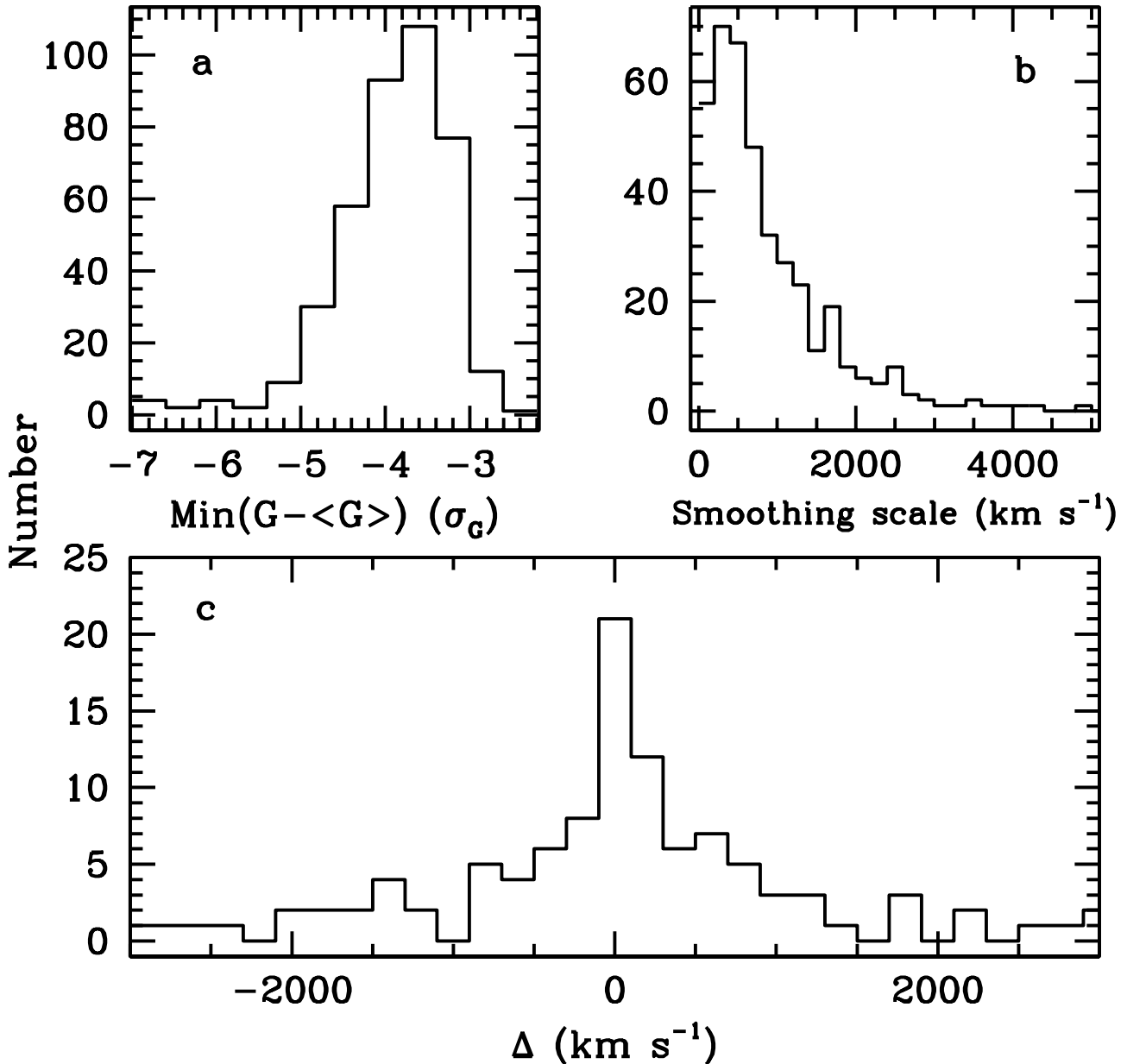


Figure 7. Distributions of (a) values and (b) scales of minima detected in reduced transmission triangles of spectra with GQED clustering. (c) Distribution of differences between the positions of the ‘strongest’ clusters (see text) and the minima of (a).

distributions of the values, positions and scales of the minima detected in the reduced averaged triangles are plotted in panels (a), (b) and (c) respectively. *All* detections are above the 3σ level and from panel (b) we see that all detections are due to the wall. Taking the top hat shape of the wall into account, its thickness has correctly been recovered in panel (c). Using the peaks of the three distributions we calculate an overdensity of 2.6 (see also Figure 6). As in Figure (8) we plot in panel (d) the distribution of the maximum values detected in the averaged two-point correlation functions using the ‘observed’ (solid line) and the ‘real’ (dotted line) line lists. In addition, we performed a *cross-correlation* analysis and show the result as the dashed histogram. Both auto- and cross-correlations fail to deliver a significant result. In fact, even with *infinite* resolution and a *perfect* line fitting algorithm, the auto-tpcf analysis does a worse job of uncovering the ‘wall’ than our analysis using intermediate resolution.

For both cases discussed above we have demonstrated that our new analysis is substantially more sensitive to the presence of non-random structure in the Ly α forest than a traditional two-point correlation function analysis when applied to

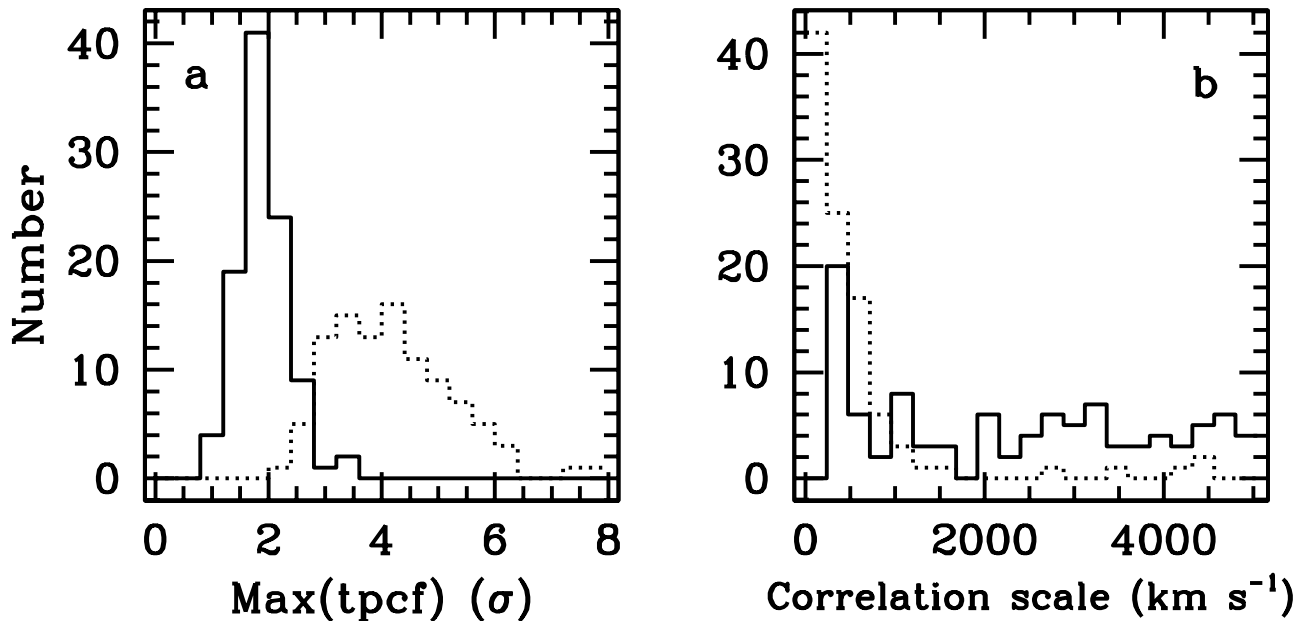


Figure 8. Distributions of (a) values and (b) correlation scales of averaged two-point correlation function maxima using ‘observed’ line lists (solid lines) and ‘real’ line lists (dashed lines).

intermediate resolution data. To further illustrate this point we show in Figure (10) the same distributions as in Figures (7), (8) and (9) for the case where absorbers are randomly distributed. We note that the distributions of transmission minima in Figures (7) and (9) differ substantially from the one in Figure (10), whereas the distributions of tpcf maxima are very similar. In panel (b) of Figure (10) we see the effect of the non-Gaussian statistics at small smoothing scales as discussed above: the minimum value in a transmission triangle is more likely to occur at small smoothing scales than at large ones which is why the minima are not evenly distributed over all scales as are the maxima of the tpcf.

4 CONCLUSIONS

In this paper we have developed a new technique to test for non-random structure in the Ly α forest. This new technique does not require line fitting but is rather based on the statistics of the transmitted flux. We have tested the relevant analytic calculations and approximations against simulated data and have found excellent agreement. We have argued that the accuracy of our method is limited by the precision of the continuum fit and by the errors in the line distribution parameters rather than by errors introduced by analytic approximations. We have shown our new analysis to be substantially more sensitive to non-randomness in intermediate resolution data than a traditional two-point correlation function analysis. Finally, we have presented evidence that, in the case of a coherent structure of absorbers extending across several lines of sight, our analysis using *intermediate* resolution data is at least comparable, if not superior, in sensitivity to a tpcf analysis using *high* resolution data.

The next step is to apply our method to real data. In a forthcoming paper we will present the results of our analysis of the spectra of a close group of ten QSOs.

REFERENCES

- Bahcall J. N. et al., 1993, ApJS, 87, 1
 Bechtold J., 1994, ApJS, 91, 1
 Bi H., Davidsen A. F., 1997, ApJ, 479, 523
 Bond J. R., Wadsley J. W., 1998, in Petitjean P., Charlot S., ed, “Structure and Evolution of the IGM from QSO Absorption Line Systems”, Proc. 13th IAP Colloquium, p. 143
 Bowen D. V., Blades J. C., Pettini M., 1996, ApJ, 464, 141
 Broadhurst T. J., Ellis R. S., Koo D., Szalay A. S., 1990, Nat, 343, 726
 Carswell R. F., Morton D. C., Smith M. G., Stockton A. N., Turnshek D. A., Weymann R. J., 1984, ApJ, 278, 486
 Cen R., Miralda-Escudé J., Ostriker J. P., Rauch M., 1994, ApJ, 437, L9

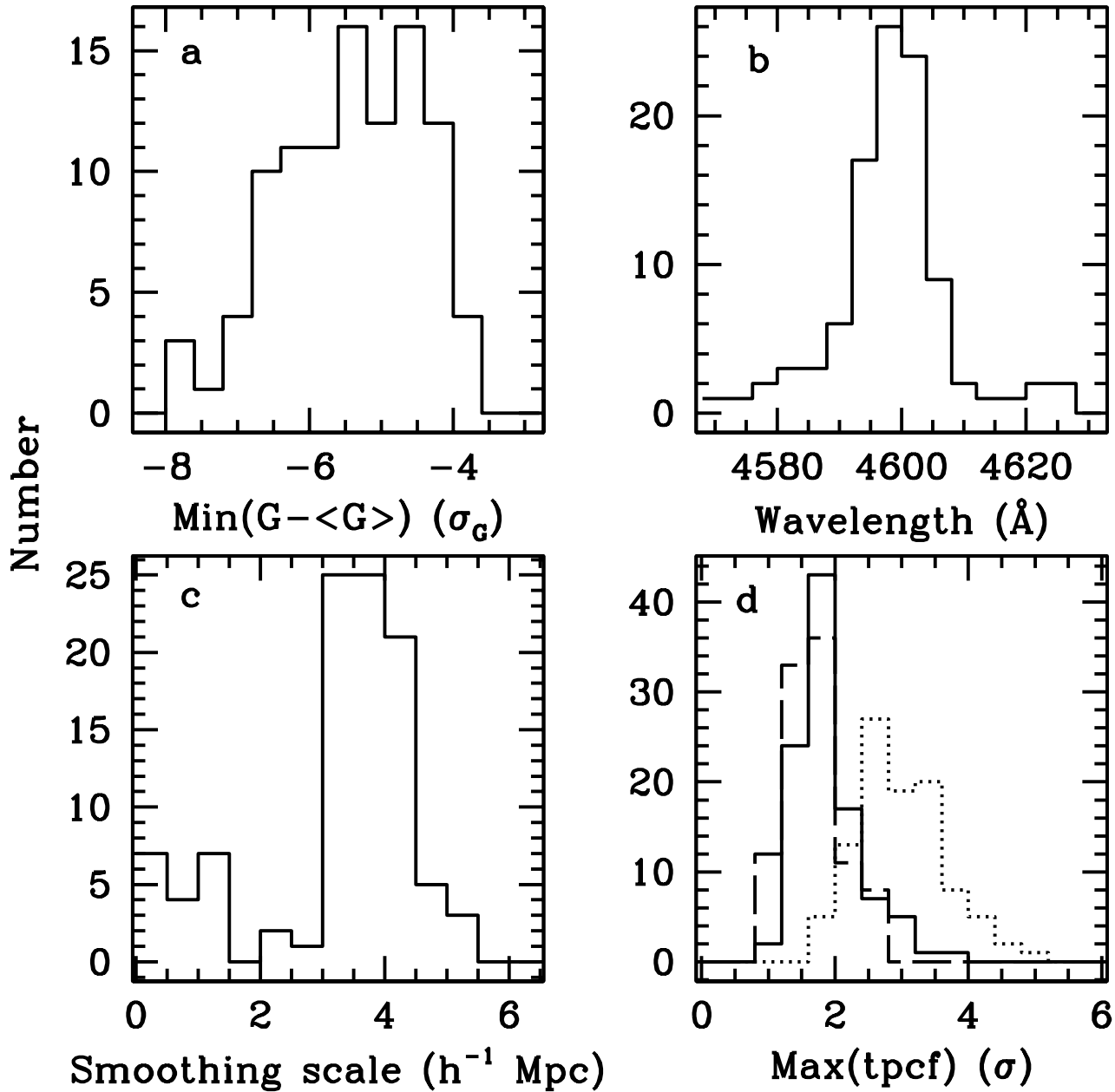


Figure 9. Distributions of (a) values, (b) positions and (c) scales of minima detected in reduced averaged transmission triangles, where absorbers form a ‘wall’ at 4600 \AA . (d) Distribution of maxima of averaged auto- (solid line) and cross-correlation (dashed line) functions using ‘observed’ and ‘real’ (auto only, dotted line) line lists.

Cen R., Simcoe R. A., 1997, *ApJ*, 483, 8
 Chen H.-W., Lanzetta K. M., Webb J. K., Barcons X., 1998, *ApJ*, 498, 77
 Connolly A. J., Szalay A. S., Romer A. K., Nichol R., Holden B., Koo D., Miyaji T., 1997, in *Proceedings of the 18th Texas Symposium in Relativistic Astrophysics*, astro-ph/9702025
 Cooke A. J., Espey B., Carswell R. F., 1997, *MNRAS*, 284, 552
 Di Nella H., Couch W. J., Paturol G., Parker Q. A., 1996, *MNRAS*, 283, 367
 Einasto J. et al., 1997, *Nat*, 385, 139
 Ettori S., Guzzo L., Tarenghi M., 1997, *MNRAS*, 285, 218
 Fernández-Soto A., Lanzetta K. M., Barcons X., Carswell R. F., Webb J. K., Yahil A., 1996, *ApJ*, 460, L85
 Gnedin N. Y., 1998, *MNRAS*, 294, 407
 Hellsten U., Davé R., Hernquist L., Weinberg D. H., Katz N., 1997, *ApJ*, 487, 482
 Hernquist L., Katz N., Weinberg D. H., Miralda-Escudé J., 1996, *ApJ*, 457, L51

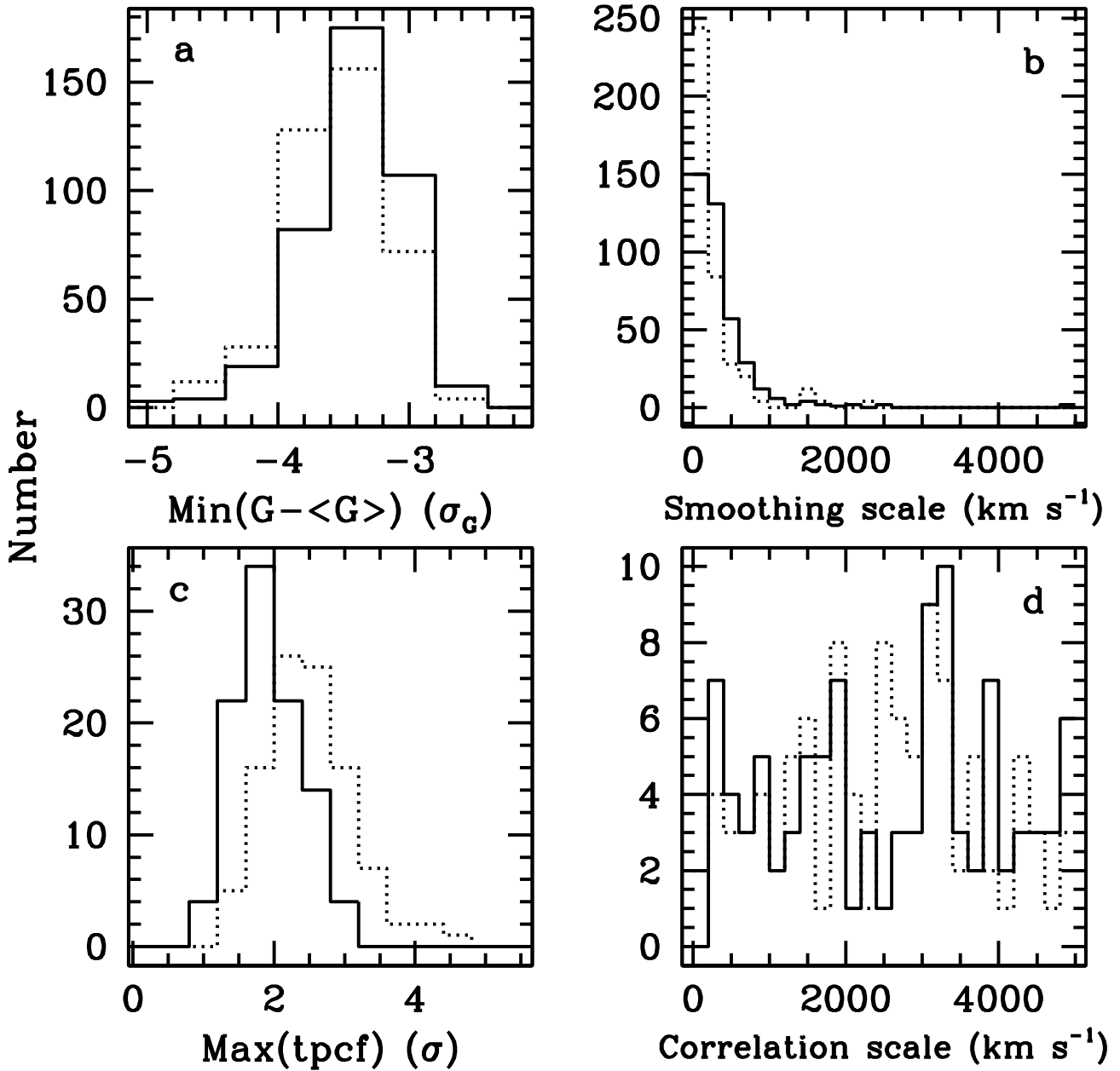


Figure 10. Distributions of (a) values and (b) scales of minima detected in reduced individual (solid lines) and averaged (dotted lines) transmission triangles, where absorbers are distributed randomly. The dotted histograms were renormalised. Distributions of (c) values and (d) correlation scales of maxima of averaged two-point correlation functions using ‘observed’ (solid lines) and true (dotted lines) line lists.

Hu E. M., Kim T.-S., Cowie L. L., Songaila A., Rauch M., 1995, *AJ*, 110, 1526
 Jenkins E. B., Ostriker J. P., 1991, *ApJ*, 376, 33
 Jenkins G. M., Watts D. G., 1968, *Spectral Analysis and its Applications*. Holden-Day, San Francisco
 Kim T.-S., Hu E. M., Cowie L. L., Songaila A., 1997, *AJ*, 114, 1
 King I. R., 1966, *AJ*, 71, 64
 Kirkman D., Tytler D., 1997, *ApJ*, 484, 672
 Lanzetta K. M., Bowen D. B., Tytler D., Webb J. K., 1995, *ApJ*, 442, 538
 Lanzetta K. M., Webb J. K., Barcons X., 1996, *ApJ*, 456, L17
 Lu L., Sargent W. L. W., Womble D. S., Takada-Hidai M., 1996, *ApJ*, 472, 509
 Lu L., Zuo L., 1994, *ApJ*, 426, 502
 Miralda-Escudé J., Cen R., Ostriker J. P., Rauch M., 1996, *ApJ*, 471, 582

- Mücket J. P., Petitjean P., Kates R. E., Riediger R., 1996, *A&A*, 308, 17
Neyman J., Scott E. L., 1952, *ApJ*, 116, 144
Oke J. B., Korycansky D. G., 1982, *ApJ*, 255, 11
Pando J., Fang L.-Z., 1996, *ApJ*, 459, 1
Petitjean P., Mücket J. P., Kates R. E., 1995, *A&A*, 295, L9
Petitjean P., Webb J. K., Rauch M., Carswell R. F., Lanzetta K. M., 1993, *MNRAS*, 262, 499
Press W. H., Rybicki G. B., Schneider D. P., 1993, *ApJ*, 414, 64
Rauch M. et al., 1997, *ApJ*, 489, 7
Riediger R., Petitjean P., Mücket J. P., 1998, *A&A*, 329, 30
Saslaw W. C., 1989, *ApJ*, 341, 588
Saslaw W. C., Hamilton A. J. S., 1984, *ApJ*, 276, 13
Sheth R. K., Saslaw W. C., 1994, *ApJ*, 437, 35
Songaila A., Cowie L. L., 1996, *AJ*, 112, 335
Tripp T. M., Lu L., Savage B. D., 1998, *ApJ*, accepted, astro-ph/9806036
Wadsley J. W., Bond J. R., 1997, in Clarke D., West M., ed, "Computational Astrophysics", Proc. 12th Kingston Conference, astro-ph/9612148
Webb J. K., Barcons X., Carswell R. F., Parnell H. C., 1992, *MNRAS*, 255, 319
Weymann R. J., Carswell R. F., Smith M. G., 1981, *ARA&A*, 19, 41
Williger G. M., Baldwin J. A., Carswell R. F., Cooke A. J., Hazard C., Irwin M. J., McMahon R. G., Storrie-Lombardi L. J., 1994, *ApJ*, 428, 574
Williger G. M., Smette A., Hazard C., Baldwin J. A., McMahon R. G., 1998, in Petitjean P., Charlot S., ed, Proceedings of the 13th IAP Colloquium "Structure and Evolution of the Intergalactic Medium from QSO Absorption Line Systems"
Zhang Y., Anninos P., Norman M. L., 1995, *ApJ*, 453, L57
Zuo L., 1993, *A&A*, 278, 343
Zuo L., Bond J. R., 1994, *ApJ*, 423, 73
Zuo L., Lu L., 1993, *ApJ*, 418, 601
Zuo L., Phinney E. S., 1993, *ApJ*, 418, 28